# A "tabletop" electrostatic ion storage ring: Mini-Ring

J. Bernard,[1] G. Montagne,[1] R. Brédy,[1] B. Terpend-Ordacière,[1] A. Bourgey,[1] M. Kerleroux,[1] L. Chen,[1] H. T. Schmidt,[2] H. Cederquist,[2] and S. Martin[1]
[1]*Université Lyon 1, CNRS, LASIM UMR 5579, bât. A. Kastler, 43 Bvd. du 11 novembre 1918, F-69622 Villeurbanne, France*
[2]*Department of Physics, Stockholm University, AlbaNova University Center, S-10691 Stockholm, Sweden*

(Received 7 April 2008; accepted 20 June 2008; published online 30 July 2008)

We report on the design, construction, and commissioning of a novel electrostatic ion storage ring of small dimensions—in the following referred to as "Mini-Ring." Mini-Ring consists of four horizontal parallel-plate deflectors and two conical electrostatic mirrors. Ions are injected through the two deflectors on the injection side and off axis with respect to the conical mirrors which face each other. The first injection deflector, originally at zero voltage, is switched to its set value such that the ions after one turn follow stable trajectories of lengths of roughly 30 cm. This design reduces the number of electrodes necessary to guide the ion beam through the ring in stable orbits. The six elements (deflectors and mirrors) are placed on a common grounded plate—the tabletop. Here, we present the design, ion trajectory simulations, and results of the first test experiments demonstrating the successful room-temperature operation of Mini-Ring at background pressures of $10^{-6}-10^{-7}$ mbar. © *2008 American Institute of Physics.* [DOI: 10.1063/1.2957609]

## I. INTRODUCTION

Since the middle of the 90s there has been a growing interest in electrostatic storage devices allowing for the storage of ion beam pulses in the energy range of 1–100 keV. An important advantage over magnetic storage is that heavy ions, such as cluster or biomolecular ions, may be stored just as conveniently as light ions (cf. Ref. 1 for a review article). The earliest examples in this context are the electrostatic ion storage ring in aarhus (ELISA) at Aarhus University in Denmark[2,3] and the (linear) electrostatic ion beam traps developed independently at the Weizmann Institute[4] and at the Lawrence Berkeley National Laboratory.[5] A few years later, a very simple linear electrostatic trap using only three electrodes was constructed at Stockholm University.[6] Two of the electrodes in the Stockholm trap are conical electrostatic mirrors and this trap was therefore named ConeTrap.[6] Two conical mirrors are also used in Mini-Ring. Several experiments with electrostatic storage devices have been devoted to measurements of lifetimes of metastable states in atomic ions,[7–9] but the experimental programs also include studies of the stabilities and fragmentations of molecular and cluster ions.[10,11] At ELISA, an electrospray ion source has been installed for studies of biomolecules, their fragmentation and their spectroscopic properties in the gas phase.[12–17] Similar studies may also be performed in Mini-Ring, which due to its small size has the additional advantage of comparatively easy cooling of the full setup to very low temperatures.

At KEK-Tsukuba, Japan, interactions between merged electron and biomolecular beams have been studied in an electrostatic storage ring[18,19] which, apart from its unique electron target, has a design very close to that of ELISA.[2,3] Another storage ring, similar in construction to the one at KEK-Tsukuba, but with the option of operation at liquid nitrogen temperature was recently commissioned at Tokyo Metropolitan University.[9] Among the electrostatic storage rings which presently are under construction, the Cryogenic Storage Ring[20] (CSR) in Heidelberg, Germany, will be the largest one with its 30 m circumference—i.e., it will be a hundred times larger than Mini-Ring. The CSR will be equipped with an ultracold electron target, a gas-jet target, and a reaction microscope, and it will have the option to merge stored ion beams with lasers or neutral atomic or molecular beams in one of its straight sections. Some sections of CSR will be cooled to 2 K. DESIREE at Stockholm University in Sweden, will be unique as it will contain *two* electrostatic storage rings (circumferences of 8.8 m) with a common section for energy fine tuning of collisions between positive and negative ions of atoms, molecules, clusters, and/or biomolecules at cryogenic temperatures.[21,22] In CSR and DESIREE, the ion storage will be used to cool internally hot molecules but it will also be possible to actively precool ions in cryogenically operated traps on the injection lines. In such ways it will be possible to control the quantum states of the stored ions before they are allowed to interact. Miniring with its small size is also, as already mentioned, suitable for experiments at extremely low temperatures although the capability to store ions is smaller than for CSR and DESIREE.

The CSR and DESIREE projects are indeed interesting, but certainly also very challenging demanding that a range of nontrivial instrumental problems are solved. For example, it was only very recently that it was shown that position-sensitive microchannel plate detectors may be used for particle counting at high rates (at least up to kilohertz) even at cryogenic temperatures.[23] Several additional problems connected with the handling of ions, ion signals, beam diagnostics, etc., remain to be solved in connection with the large cryogenic rings. Thus, the much smaller Mini-Ring project (in terms of cost, size complexity, etc.) is extremely suitable for gaining experience with different technical solutions and

 

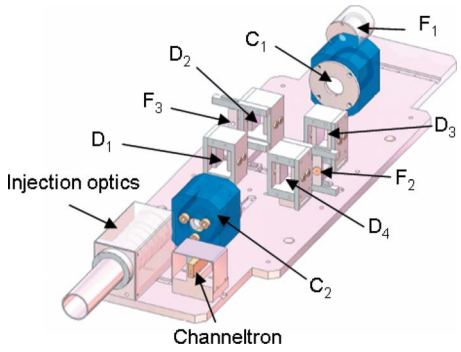


FIG. 1. (Color online) A three dimensional scale drawing of Mini-Ring. The ion optical elements—two conical mirrors and four deflectors are carefully positioned (precision of the order of 0.1 mm) on a common mounting plate. The conical mirrors are labeled $C_1$ and $C_2$, the four parallel-plate deflectors $D_1$–$D_4$ are shown in their grounded housings, and $F_1$–$F_3$ are the three Faraday cups used for diagnostics (cf. text).

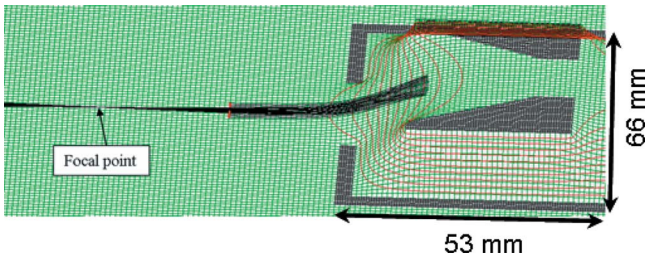


FIG. 2. (Color online) Results of ion optical simulation of trajectories in a single conical mirror. The focal point is indicated for $\xi_m = qV_m/E_k = 1.35$ where $q$ is the ion charge state, $V_m$ is the mirror voltage, and $E_k$ is the kinetic energy of the ion before it enters the mirror (cf. text).

for pioneering experiments on lifetimes and stabilities of simple and complex ions in situations where control of the internal excitations of the stored ions may be achieved. The stability of highly charged positive $C_{60}$ ions was studied using a specially designed version of ConeTrap at the University of Lyon[24,25] and this work, and ConeTrap[6] itself, has been part of the inspiration for the present ring development. Miniring (which may be contained in a standard vacuum chamber) makes use of the focusing properties of two conical electrodes, but here the stored ion trajectories also traverse two sets of double horizontal deflectors. In Mini-Ring, ions are injected off axis and through one of the horizontal deflector sets while they are injected through holes in the cones in ConeTrap.

In this work, we report results from the first test experiments demonstrating the successful operation of Mini-Ring under modest vacuum conditions. We demonstrate the storage of $Ar^+$- and $He^+$-ion beams of 2–4 keV with millisecond lifetimes at $10^{-6}$–$10^{-7}$ mbar. As the comparison between the present Mini-Ring results for the lifetime of a 2 keV $Ar^+$ beam and corresponding results with ConeTrap at lower pressure indicate that the background gas is the limiting factor, we foresee that ion storage times will be increased substantially for lower background pressures in Mini-Ring.

## II. DESIGN ASPECTS FOR MINIRING

The mechanical design of Mini-Ring is shown in Fig. 1. Miniring has two conical mirrors inside grounded shieldings and in addition four parallel-plate deflectors inside their separate grounded shields. Injection optics is used for fine tuning of the entrance angle, entrance position, and focusing of the beam. We use three Faraday cups and a channeltron detector for diagnostics. The current measurement with Faraday cup $F_1$ (see Fig. 1) is used in order to tune the incoming beam. When the bias for storage is applied to deflector $D_2$ and the conical mirror $C_1$, the ion beam will hit Faraday cup $F_2$ as long as no voltage is applied to $D_3$. Likewise, if voltages for ion storage are applied to the elements $D_2$, $C_1$, $D_3$, $D_4$, and $C_2$ while $D_1$ is kept at zero, the ion beam will hit Faraday cup $F_3$ after one turn. The mechanical parts of Mini-Ring are placed on a single mounting plate (see Fig. 1) for positioning with a precision of 0.1 mm.

We will now go on to describe the optical properties of the two basic ion optical elements of Mini-Ring—the conical mirror and the horizontal deflector. The focal properties of conical electrostatic mirrors have been described in detail in earlier papers on ConeTrap[6,24] and similar, although not identical, mirrors are used in Mini-Ring. In Ref. 6, the dependence of the focal length on the voltage on one isolated conical electrode is calculated (simulated) and the result explains the observation of two cone-voltage regions for stable ConeTrap operation. In Mini-Ring, the conical electrodes have larger angles than in ConeTrap in order to increase the acceptances of the mirrors for off axis trajectories. Ion trajectory simulations (with SIMION 8.03) have been performed in order to optimize the design of the conical electrodes and their grounded housings. In order to obtain stable orbits in linear beam traps,[6,24] it is necessary that $L_x/4 \leqslant f_m < \infty$, where $f_m$ is the focal distance of the mirrors and $L_x$ is the distance between the mirror electrodes (entrances of the cones in the case of ConeTrap). Let us now, for a single conical mirror, define the dimensionless parameter $\xi_m = qV_m/E_k$ where $q$ is the charge state of the ion, $V_m$ is the voltage on the conic electrode, and $E_k$ is the kinetic energy of the ion far away from the cone. In Fig. 2, we show the position of the focal point for one conical Mini-Ring mirror with its housing for the case $\xi_m = 1.35$. In Fig. 3, we show the focal distances, $f_m$, as functions of $\xi_m$ and we find a strong increase when approaching $\xi_m = \xi_{\max} = 1.4$. When $\xi_m > \xi_{\max}$, the mirror is defocusing and, thus, $\xi_{\max}$ is an upper limit for stable Mini-Ring ion trajectories.

The deflectors in Mini-Ring are used in order to be able to inject the ion beam off axis with respect to the conical mirrors. As mentioned above, the parallel-plate deflectors were placed inside their rectangular grounded housings. The latter are used to terminate the electrical fields in the beam direction. For stable trajectories, the focal distances of the horizontal deflectors should fulfil the condition $L_y/4 \leqslant f_{D_y} < \infty$, where $L_y = 80$ mm is the distance between central trajectories through the horizontal deflectors on the injection side ($D_1$ and $D_2$) and on the opposite side ($D_3$ and $D_4$) and $f_{D_y}$ is the focal length in the horizontal plane. We now define a second dimensionless parameter $\xi_D = q(V_{D+} - V_{D-})/2E_k$, where $V_{D+}$ and $V_{D-}$ are the positive and negative plate voltages. The deflection angle depends linearly on $\xi_D$. As an

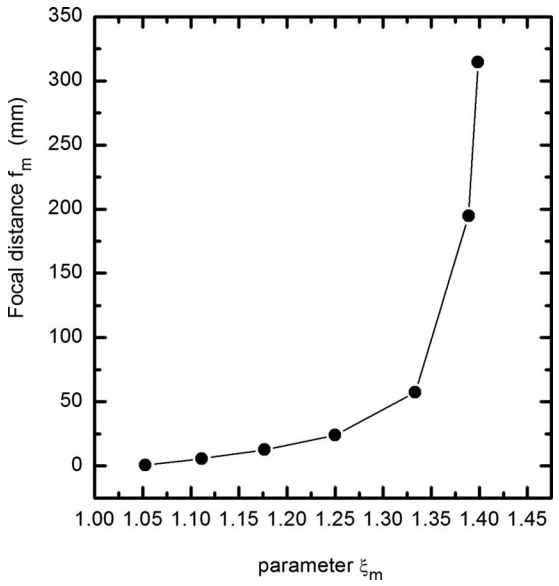


FIG. 3. Ion optical simulations of the focal positions as functions of $\xi_m = qV_m/E_k$ (cf. text).

example, we show an ion trajectory simulation for $\xi_D = 0.16$ and the position of the focal point for one deflector in Fig. 4. In Fig. 5, we show the positions of the focal points $(F_x, F_y)$ for a single horizontal deflector as functions of $\xi_D$ (see Fig. 4 for a definition of the coordinate system). The deflector focuses in the horizontal direction only and has no focusing effect in the vertical direction, while the conical mirrors focus in the same way in both directions. Consequently the net focusing effects for the whole Mini-Ring system are different in the plane of the ring and in the perpendicular direction. However, in order to get stable trajectories, the focusing conditions must be fulfilled in both the vertical and horizontal directions for the complete ion optical system of Mini-Ring. With ion trajectory simulations, Mini-Ring geometries which fulfil these conditions for focusing have been identified. The distance between the two mirrors in Mini-Ring is 294 mm and the centers of the horizontal deflectors have been placed at distances of $L_y/2 = 40$ mm off the central axis of the conical mirrors. With this geometry, the deflection angle for stable ion storage is close to 18° with 0° entrance angles in the deflectors $D_2$ and $D_4$. For deflectors $D_3$ and $D_4$, the entrance angle is 18°, nevertheless, trajectory simulations show that the focal distances are the same.

## III. ION TRAJECTORY SIMULATIONS

We have, in addition to what has been described above, performed ion trajectory simulations in order to validate and

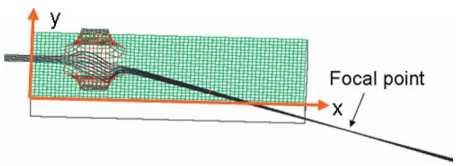


FIG. 4. (Color online) Ion optical simulations of trajectories (black curves) in a single parallel-plate deflector. Equipotential curves are indicated. The focal point is shown for $\xi_D = q(V_{D+} - V_{D-})/2E_k = 0.16$ (cf. text).

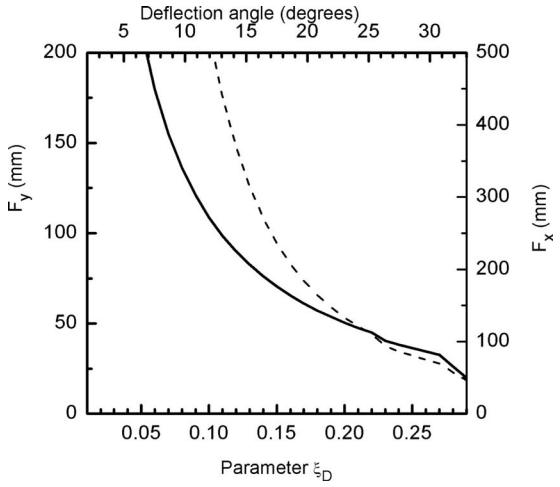


FIG. 5. The $x$ and $y$ coordinates for focal positions for a single parallel-plate deflector as functions of $\xi_D = q(V_{D+} - V_{D-})/2E_k$. The dashed curve and the right hand scale and the full curve and the left hand scale give the $x$ and $y$ positions, respectively.

to further characterize the Mini-Ring design. In Fig. 6, we show an ideal ion trajectory calculated for 1 keV $Ar^+$ ions with zero transversal velocity components in the middle of the gap between the horizontal deflectors. For this simulation, ions were launched at coordinates $(x,y,z) = (0,40,0.5)$ mm and the potentials of the conical mirrors and the deflector plates have been set to $V_m = 1340$ V $(\xi_m = 1.34)$ and $V_D = 160$ V $(\xi_D = 0.16)$, respectively. In order to determine the sensitivities to these settings, $V_m$ and $V_D$ (and hence, $\xi_m$ and $\xi_D$) have been varied. This was also done in order to identify the limiting values for stability. The region of stability in the $(\xi_m, \xi_D)$ plane is given by the area enclosed by the square symbols in Fig. 7, while the open circles give the $(\xi_m, \xi_D)$ coordinates for stored beams in actual test experiments which will be described in detail in the following section. The shape of the stability region is given by the geometry of the ring including, of course, the distance between the conical mirrors and the positions of the deflectors. We note that the values of $V_m$ and $V_D$ may vary over fairly large ranges while still maintaining stable ion-beam trapping in Mini-Ring. As expected, trajectories remain closer to the ideal orbit of Fig. 6 when $\xi_m$ and $\xi_D$ remain close to the center of the stability region of Fig. 7. Moreover, it can be expected that, for a "real" beam with a spread in ion injection

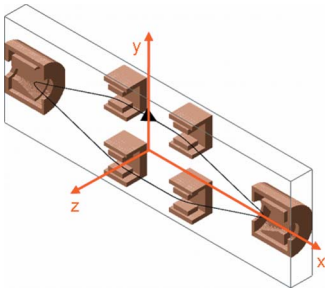


FIG. 6. (Color online) Three dimensional ion optics simulation of an ion trajectory for 1 keV $Ar^+$ in Mini-Ring. The black arrow shows the starting point and starting direction (parallel to the $x$ axis) of the trajectory. The voltage of the conical electrodes is 1340 V and the voltages on all four deflectors are ±155 V (giving $\xi_m = 1.37$ and $\xi_D = 0.155$).

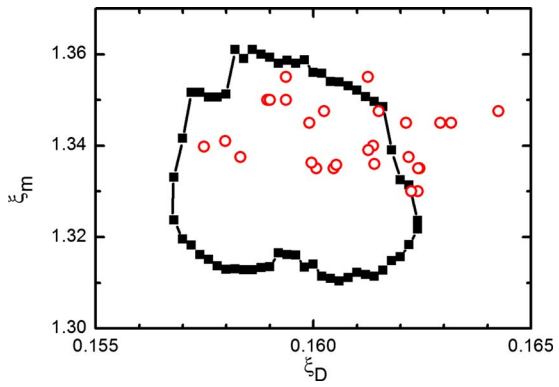


FIG. 7. (Color online) The region for stable ion trajectories in Mini-Ring as calculated by means of ion optical simulations (squares) are expected to lie in the $(\xi_m, \xi_D)$ plane and inside the area defined by the squares connected by straight lines. Open circles: experimental values of $\xi_m$ and $\xi_D$ for which ion beams have been successfully trapped in the Mini-Ring for at least several hundreds of microsecond.

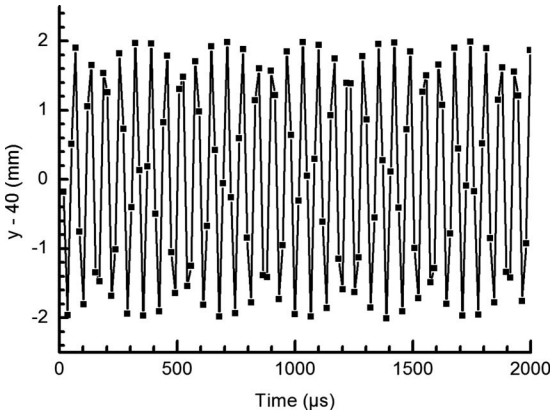


FIG. 9. Squares: simulated $y$ positions for ions passing through the $yz$ plane at $x=0$ (coordinate system defined in Fig. 6) for 1 keV $Ar^+$ ions with $\xi_m=1.34$ and $\xi_D=0.155$ which is at the center of the stability region in the $(\xi_m, \xi_D)$ plane. The period for the betatron oscillations is $T_\beta=38.8$ $\mu$s while the revolution time is 10.7 $\mu$s.

angles and positions, the trapping efficiency may decrease continuously from 1 to 0 near the limit of the stability region. This more complete study has yet to be completed and will be presented in a forthcoming paper.

We have also performed simulations in order to estimate the maximum emittance of a stable, circulating, beam in Mini-Ring. The parameters $\xi_m$ and $\xi_D$ have then been chosen close to the center of the stability diagram. In these simulations, ions were started from a suitable region in the $yz$ plane at $x=0$ (see Fig. 6). For each initial $y$ position, the initial azimuth angle $\alpha_y$ was varied in order to find the corresponding limit for stability. The results are shown in a phase space diagram [Fig. 8(a)], where the limiting angles, $\alpha_y$, are plotted as functions of $y$. Similar simulations have been performed for the $z$ direction and the corresponding stability region in the $(z, \alpha_z)$ plane is shown in Fig. 8(b). The ellipses in Fig. 8 have been fitted to the simulated $(y, \alpha_y)$ and $(z, \alpha_z)$ data, yielding acceptances of $200\pi$ mm×mrad and $82\pi$ mm ×mrad, respectively. However, as can be seen in Fig. 8(a) there is a cutoff at $y=36$ mm as such trajectories hit the inner electrodes of the horizontal deflectors according to the simulations. We note that the shape of the stability region (cf. Fig. 7) does not depend much on the initial $y$ and $z$ positions of the launched ions, provided that they fit inside the acceptance of the Mini-Ring (cf. Fig. 8).

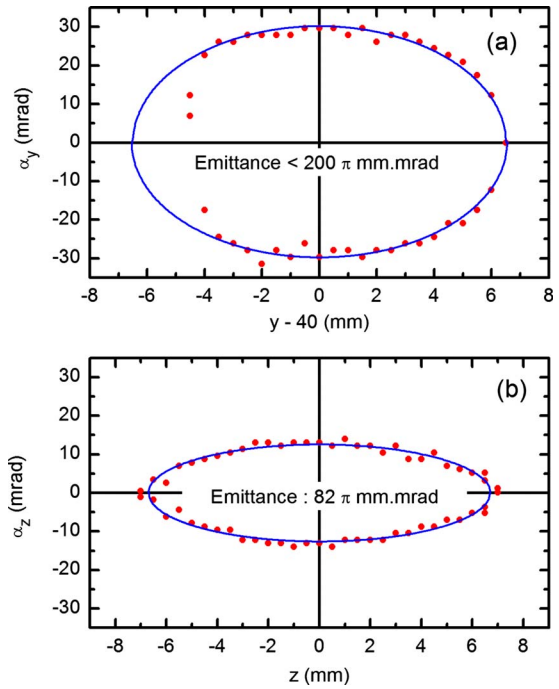


FIG. 8. (Color online) Phase space diagrams for ion beam acceptance in Mini-Ring in $y$ and $\alpha_y$ (a) and in $z$ and $\alpha_z$ (b). Beams with emittances inside the regions defined by the calculated acceptance limits (data points) are expected to be stored. We also show fitted ellipses which approximately describe the areas within which ion beams are accepted in Mini-Ring.

It is also instructive to study the ion movement in the directions perpendicular to the circulating ion beam. As already mentioned, the focal properties of Mini-Ring are different in the horizontal $(y)$ and the vertical $(z)$ directions. In one simulation, a 1 keV $Ar^+$ ion has been launched from $(x,y,z)=(0.00,0.43,0.00)$ mm with the velocity vector parallel to the $x$ axis. In Fig. 9 we show the $y$ positions for the passages through the $yz$ plane at $x=0$—i.e., the betatron oscillations. For 1 keV $Ar^+$ ions, the period of these oscillations is 38.8 $\mu$s while the revolution period is 10.7 $\mu$s. Similar betatron oscillations appear also in the vertical dimension but in this case with a period of 35.8 $\mu$s. It is easy to verify with the simulations that the periods of these movements scale with the initial velocity of the stored particles, i.e., with the square root of the initial energy and with the inverse of square root of the mass. Additional simulations show that larger initial displacements (of up to 2 mm) of the trajectory from $y=0$ or $z=0$ increase the amplitude of the betatron oscillations while the frequencies are not significantly affected.

## IV. FIRST OPERATION OF MINIRING

### A. Detection of photons and neutrals

Ion beams of $Ar^+$ and $He^+$ from a NanoGan 3 ECR ion source have been injected in Mini-Ring for tests and commissioning purposes at room temperature. These ion beams were accelerated to 2 or to 4 keV and selected according to their mass to charge ratios in a DanFysik accelerator. The ion

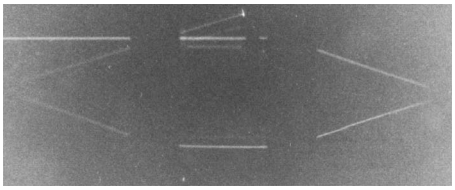

FIG. 10. A photograph of the ion-beam track of 200 nA $Ar^+$ in Mini-Ring while deliberately letting in $N_2$ gas to give a pressure of $2\times10^{-4}$ mbar. The beam current was measured in the Faraday cup $F_3$ after one turn. The photograph was taken using a reflex camera (focal length of 24 mm, diaphragm of 5.6) with a black and white 1600 ASA film ($24\times36$ mm$^2$) and 10 h exposure time.

beam intensities were measured by means of a Faraday cup $F_3$ (see Fig. 1) after single turns in Mini-Ring and were about 200 nA both for $Ar^+$ and $He^+$ (at 4 keV). In Fig. 10, we show a photograph of repeated, single turns, 4 keV $Ar^+$ ion beams in Mini-Ring. In order to obtain sufficient light intensities, we increased the pressure in the vacuum chamber by letting in $N_2$ gas. Collisions between the ion beam and $N_2$ then gave sufficient photon intensities for manageable exposure times (typically 10 h). As seen from the photograph, the intensity decreases along the beam trajectory due to neutralization and beam loss processes at the present elevated pressures. In the dark sections the beam passes through ion optical elements and their shields and, consequently, photons coming from those sections could not be detected. A support for the faraday cup $F_3$ blocks the line of sight to the beam in the upper horizontal section near the deflector $D_2$. It is also interesting to note that the light intensity is smaller at the turning points near the conical mirrors presumably due to smaller cross sections at lower velocities.

During the commissioning of Mini-Ring, several voltage combinations for the conical mirrors and the deflectors have been tested. That is, the $\xi_m$ and $\xi_D$ parameters have been varied with the aim to optimize operating conditions. The $(\xi_m, \xi_D)$ test values have been plotted in the stability diagram of Fig. 7. The agreement between the stability region obtained from ion optical simulations and the empirical values for ion-beam storage is rather good although not perfect. Deviations (i.e., stable beam observed outside the simulated stability region) are attributed to limitations in mechanical constructions and alignments and also, in some cases, to short observation times (200 $\mu$s for the shortest to 2 ms for the longest observation times).

The continuous ion beams provided by the Danfysik accelerator were pulsed before injections. The beam pulses were 1 $\mu$s long and the repetition period was 10 ms. The signal to the beam chopper was delayed and used as a trigger for the fast high voltage switches for the $D_1$ deflector. This delay was tuned such that a beam pulse could pass through $D_1$ without being deflected on its first passage. During the following turns, the same beam pulse was deflected by $D_1$ to its stable orbit. In these tests, the pressure was ranging from about $2\times10^{-7}$ to about $2\times10^{-6}$ mbar (different for different test experiments) and collisions with the residual gas lead to neutralization of trapped ions. For neutralization events along the straight section between $D_3$ and $D_4$, the neutral products were detected by means of a channeltron detector in the forward direction (see Fig. 1). The signal from the channeltron was amplified, converted to transistor-transistor logic (TTL) by a constant fraction discriminator and sent to a digital oscilloscope recording the intensity of neutrals as functions of time.

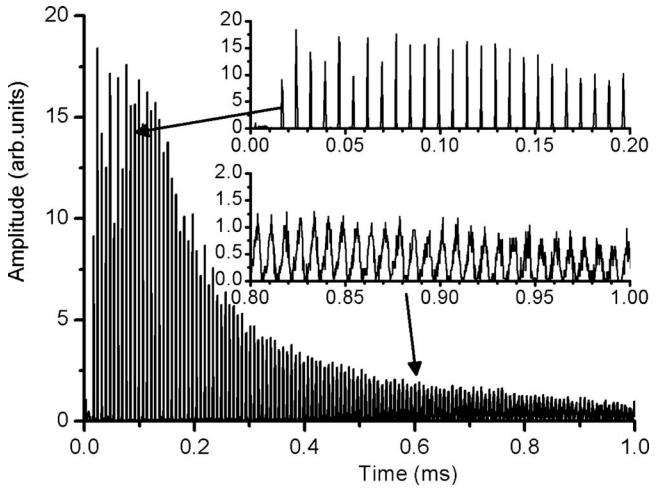


FIG. 11. Rates of neutrals from charge exchange collisions with the residual gas for a stored beam of 2 keV $Ar^+$ ions, measured as a function of storage time and by means of a channeltron detector. The zoom ins of the insets reveal the pulsed structure of the stored beam and the increase in beam pulse widths with storage time.

In Fig. 11, we show a typical time spectrum recorded over a 1 ms time range for 2 keV $Ar^+$ ions stored in Mini-Ring. The structure in the time spectrum is due to the pulsed structure of the stored ion beam. A temporal broadening of the beam pulses as a function of storage time is seen in the insets of Fig. 11. This broadening is caused by the energy spread in the injected ion beam pulses and by different trajectory lengths due to the finite dimension of the incoming beam. Elastic scattering with the residual gas could also play a role but this effect is probably less important. Intrabeam scattering gives a very small contribution as the stored ion beam intensity was strongly reduced in order to avoid saturation of the detector when it was operated in the single-particle counting mode. The integrated intensities of the beam-pulse peaks in Fig. 11 are displayed in Fig. 12 as func-

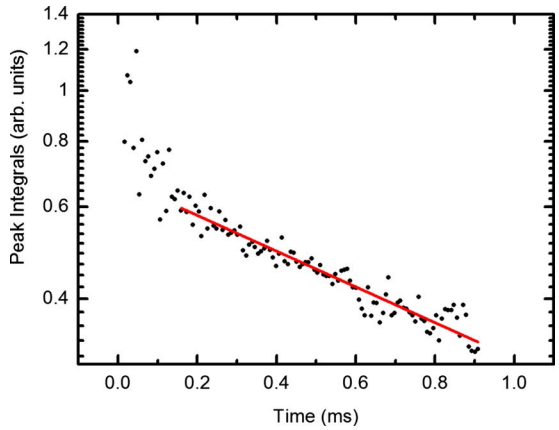


FIG. 12. (Color online) Integrated intensities of neutrals produced by the ion beam pulses as functions of the storage time (the intensities in the peaks in Fig. 11 have been integrated). Full red curve: fit to an exponential decay.

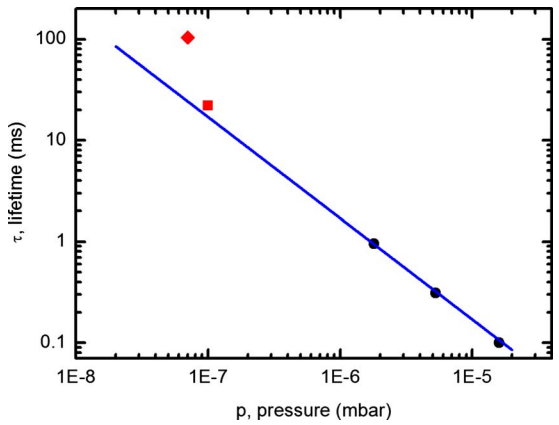


FIG. 13. (Color online) Filled circles: measured lifetimes for 2 keV $Ar^+$ ions in Mini-Ring at three different gas pressures. Diamond: measured lifetime of 4 keV Ar ions in the Stockholm ConeTrap (Ref. 6). Square: measured lifetime of 600 eV $Ar^+$ ions in the Lyon ConeTrap (Ref. 25). Full line: a linear fit ($\tau=\alpha/p$) to the Mini-Ring data.

tions of the storage time. In the beginning, a fast decay is observed due to the loss of ions with unstable trajectories. Then, a slower decay with a lifetime of about 1 ms is observed and this part is attributed to collisions with the residual gas (in this case at a pressure of $1.6\times10^{-6}$ mbars). Fig. 13 shows results of lifetime measurements with 2 keV $Ar^+$ ion beams in Mini-Ring at three different pressures, and corresponding results for 4 keV $Ar^+$ and 600 eV $Ar^+$ beams in ConeTrap at lower pressures (the latter results are from Stockholm and Lyon, respectively). The Mini-Ring results are well described by a $\tau\sim1/p$ scaling law (where $\tau$ is the lifetime and $p$ is the pressure in mbar). The extrapolation of this fit toward lower pressures agrees rather well with the Stockholm and Lyon data for ConeTrap although the different energies for ion storage as well as possible differences in pressure gauge calibrations may play a role here. Still, these results strongly indicate that good storage conditions for Mini-Ring indeed has been found in the present study and that much longer lifetimes may be expected at lower background pressures.

Betatron oscillations have been observed in the case of 4 keV $Ar^+$ for which the data were recorded under conditions such that the voltage settings of the Mini-Ring were not perfectly optimized (see Fig. 14, which displays the amplitudes of peaks similar to the ones in Fig. 11 but not shown here). Below 0.3 ms, there is a series of rather strongly damped oscillations, but after 0.3 ms a smooth decay curve is recorded. The same oscillations are also clearly exposed in the fast fourier transform (FFT) spectrum of the raw spectrum in Fig. 15. The FFT spectrum has a center frequency of $F_0=188.0\pm0.6$ kHz with high intensity corresponding to the revolution frequency of 4 keV $Ar^+$ ions. In addition, there are side bands due to amplitude modulations at frequencies close to 188+50 and 188−50 kHz. These 50 kHz shifts correspond to the oscillation frequency of the measured peak amplitudes in Fig. 14. In order to discuss this point further and to determine the damping for times smaller than 0.3 ms, the experimental intensities have been fitted to

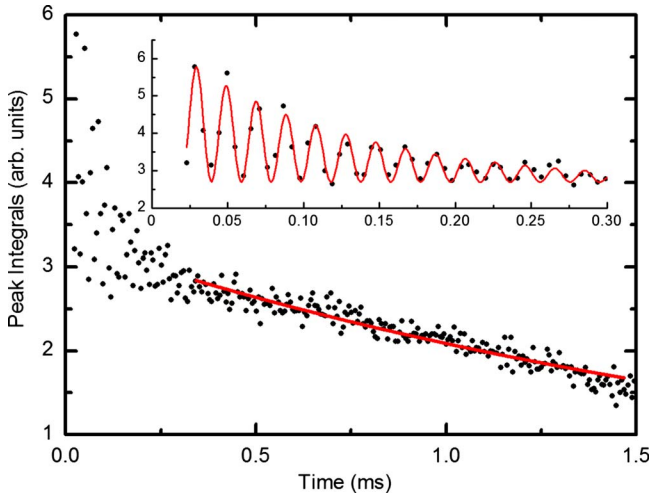


FIG. 14. (Color online) Integrated intensities of neutrals measured for 4 keV $Ar^+$ ions in conditions where the Mini-Ring voltages were not optimally set. In the time interval up to 0.3 ms, a strong oscillation is observed. Inset: the data in the time interval up to 0.3 ms is well described by Eq. (1) in the main text. The oscillation frequency of 50.8 kHz is attributed to the betatron oscillations and their influences on the probabilities for neutralized ions to hit the channeltron detector. Full red curve: fit to an exponential decay.

$$I(t)=A\cos^2(\pi F_m t+\phi)\exp(-t/\tau_1). \quad (1)$$

The inset in Fig. 14 shows a good agreement between the experimental data and this fit function for an amplitude oscillation frequency of $F_m=50.8\pm0.6$ kHz. This is consistent with the positions of the side bands in the FFT spectrum. We now compare the presently measured ratio of the fundamental frequency to the shift $r_m=F_0/F_m=188/50=3.76$ with the simulated ratio between the revolution, and betatron oscillation, frequencies which is $r_m=38.8/10.7=3.63$. This strongly indicates that the observed intensity variations of detected neutrals at short storage times are due to betatron oscillations as the probability for neutrals to hit the channeltron simply depends on how the ion trajectories pass through the horizontal deflectors of the straight section. This causes the rate of neutrals to vary from turn to turn.

The damping time has been determined from the fit of Eq. (1) using the value $\tau_1=0.11$ ms. We found that the damp-

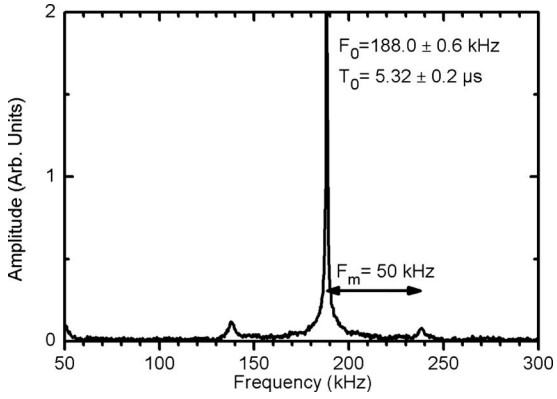


FIG. 15. FFT of the time spectrum of Fig. 14. The spectrum is typical for an amplitude-modulated signal. The center frequency is given by the revolution frequency for the stored ions. The side bands are due to the betatron oscillations.

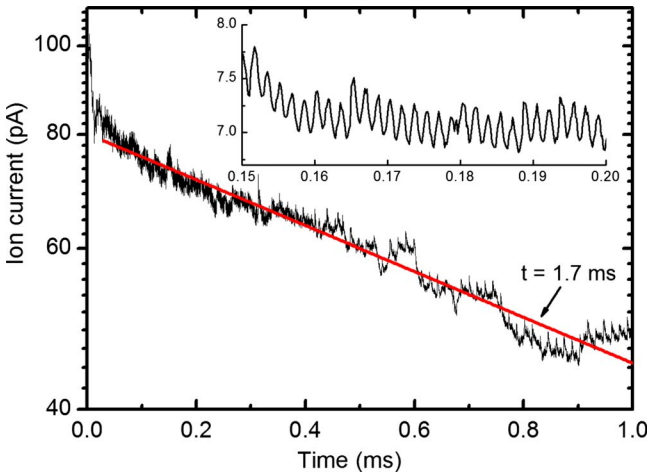


FIG. 16. (Color online) Decay curve for 4 keV $He^+$ ions stored in Mini-Ring, obtained by dumping the stored ion current on the Faraday cup $F_3$ at different times after injection (cf. text).

ing time depends on the collimation of the beam before injection such that a more well defined injected beam gave a slower initial decay of the stored ion beam intensity. By varying the emittance of the injected beam by means of different collimators before injection, it may thus be possible to get a handle of the acceptance of Mini-Ring and to compare such measurements with the corresponding simulations shown in Fig. 8. Losses of stored ions in the 0.3–1.5 ms time interval of Fig. 14 are most likely dominated by residual gas collisions (in this case the pressure was $4\times10^{-7}$ mbar). The beam intensity as a function of time has been fitted with an exponential function yielding a lifetime of around 2 ms.

### B. Ion current measurements

We have, in addition, performed test measurements of the ion storage capability of Mini-Ring by the injection of beam pulses, which ideally should contain the same numbers of ions from pulse to pulse, and by measuring the remaining current after different preset storage times. The remaining beam currents were measured by switching deflector $D_1$ to zero voltage before the arrival of the beam pulse and by integrating the current on the Faraday cup $F_3$ just behind $D_1$ (see Fig. 1). The ion beam current on Faraday cup $F_3$ was measured with a picoamperemeter and the 0–10 V output of this meter was digitized and recorded by means of a National Instrument data acquisition PCI card (NI 6221) and a PC. The storage time was controlled by the PC and measurements were performed over a range of 1 ms in steps of 0.167 $\mu$s giving spectra with 6000 channels. For each channel, the data were averaged over 20 beam-pulse injections in order to reduce the influence from beam intensity fluctuations. However, there were still some remaining variations with longer time constants which could not be averaged out. In Fig. 16, we display typical raw data in this case for a pulsed 4 keV $He^+$ beam with a pulse duration of 500 ns and a time between pulses of 1.1 ms. The long-time beam intensity variations are partly responsible for the oscillatory behavior seen in the inset of Fig. 16. In addition, the opening for Faraday cup $F_3$ is rather small (3 mm in diameter) and in cases when the $D_1$ voltage was switched with the ion pulse (partly) inside this deflector the full pulse current could not be measured. From the frequency of these latter oscillations, we deduce a revolution frequency of $594.7\pm1.2$ kHz for the present $He^+$ ions at the (nominal) injection energy of 4 keV. This is consistent with the result of $188.0\pm0.6$ kHz for the 4 keV $Ar^+$ beam (also nominal energy) when taking the different masses of He and Ar into account. From Fig. 16, we estimate that about $1.6\times10^6$ ions were injected in the Mini-Ring and that about $8\times10^5$ of them remained after 1 ms. Clearly, further test measurements with Mini-Ring will be needed to fully establish the optimal settings for ion storage at longer times, in particular, at lower pressures and lower temperatures. Still, the present early test results shows that the Mini-Ring design is successful and that much longer storage times should be expected with more favorable background pressures.

## V. CONCLUSION

In this article, we have presented the design, construction, and commissioning of a novel electrostatic storage ring, Mini-Ring, which is of true tabletop dimensions. The small dimensions have definite advantages concerning the cost, the possibility for easy operations at liquid-$N_2$ and cryogenic temperatures, the portability to different research infrastructures such as, e.g., advanced ion sources, synchrotron, or X-FEL facilities. The initial test experiments, which have been reported here, clearly demonstrate that ion beams may be stored in Mini-Ring with lifetimes of at least milliseconds at residual gas pressures in the $10^{-7}$ mbar range. Further test experiments under better vacuum conditions, and at lower temperatures, are presently being planned. We have shown that about $10^6$ ions per pulse can be stored in the Mini-Ring although in the present tests this number was limited by the intensity available from the ion source in combination with the beam transport system. For a more stringent test of the beam storage capability higher ion beam intensities are needed for injection within the Mini-Ring acceptance. The scientific program at Mini-Ring involves plans for measurements of lifetimes of long-lived states in atomic, molecular, and cluster ions and, in some cases, it is highly advantageous if such measurements can be performed at very low temperatures in order to minimize the influence from blackbody radiation from the walls of the vacuum vessels. A low temperature also has the advantage that it leads to a better vacuum through cryogenic pumping and thus longer lifetimes for stored ions making studies of important processes with low rates more attractive. Examples of planned experiments involve measurements of lifetimes of multiply charged positive ions of fullerenes, lifetimes of fullerene dianions (cf. Refs. 26 and 27), and the lifetime of the $1s2s2p\ ^4P_{5/2}$ level of $He^-$. Another attractive possibility is to study the decay and stability of laser excited ions of complex molecules such as, for instance, biomolecules.

## ACKNOWLEDGMENTS

The support received by the European Project ITS LEIF (No. RII3/026015) was gratefully acknowledged.

[1] L. H. Andersen, O. Heber, and D. Zajfman, J. Phys. B **37**, R57 (2004).
[2] S. P. Moller, Nucl. Instrum. Methods Phys. Res. A **394**, 281 (1997).
[3] J. U. Andersen, P. Hvelplund, S. B. Nielsen, S. Tomita, H. Wahlgreen, S. P. Moller, U. V. Pedersen, J. S. Forster, and T. J. D. Jorgensen, Rev. Sci. Instrum. **73**, 1284 (2002).
[4] D. Zajfman, O. Heber, L. Vejby-Christensen, I. Ben-Itzhak, M. Rappaport, R. Fishman, and M. Dahan, Phys. Rev. A **55**, R1577–R1580 (1997).
[5] W. H. Benner, Anal. Chem. **69**, 4162 (1997).
[6] H. T. Schmidt, H. Cederquist, J. Jensen, and A. Fardi, Nucl. Instrum. Methods Phys. Res. B **173**, 523 (2001).
[7] U. V. Pedersen, M. Hyde, S. P. Moller, and T. Andersen, Phys. Rev. A **64**, 012503 (2001).
[8] A. Wolf, K. G. Bhushan, I. Ben-Itzhak, N. Altstein, D. Zajfman, O. Heber, and M. L. Rappaport, Phys. Rev. A **59**, 267 LP (1999).
[9] S. Jinno, T. Takao, K. Hanada, M. Goto, K. Okuno, H. Tanuma, T. Azuma, and H. Shiromaru, Nucl. Instrum. Methods Phys. Res. A **572**, 568 (2007).
[10] V. Lepere, I. M. Ismail, M. Barat, J. A. Fayeton, Y. J. Picard, K. Wohrer, C. Jouvet, and S. Martrenchard, J. Chem. Phys. **123**, 174307 (2005).
[11] P. A. Orr, I. D. Williams, J. B. Greenwood, I. C. E. Turcu, W. A. Bryan, J. Pedregosa-Gutierrez, and C. W. Walter, Phys. Rev. Lett. **98**, 163001 (2007).
[12] I. B. Nielsen, L. Lammich, and L. H. Andersen, Phys. Rev. Lett. **96**, 018304 (2006).
[13] S. Boyé, H. Krogh, I. B. Nielsen, S. U. Pedersen, U. V. Pedersen, L. H. Andersen, A. F. Bell, X. He, and P. J. Tonge, Phys. Rev. Lett. **90**, 118103 (2003).
[14] L. H. Andersen, A. Lapierre, S. B. Nielsen, I. B.Nielsen, S. U. Pedersen, U. V. Pedersen, and S. Tomita, Eur. Phys. J. D **20**, 597 (2002).
[15] B. Liu, P. Hvelplund, S. B. Nielsen, and S. Tomita, Phys. Rev. A **74**, 052704 (2006).
[16] S. B. Nielsen, A. Lapierre, J. U. Andersen, U. V. Pedersen, S. Tomita, and L. H. Andersen, Phys. Rev. Lett. **87**, 228102 (2001).
[17] S. B. Nielsen, J. U. Andersen, J. S. Forster, P. Hvelplund, B. Liu, U. V. Pedersen, and S. Tomita, Phys. Rev. Lett. **91**, 048302 (2003).
[18] T. Tanabe, K. Noda, M. Saito, S. Lee, Y. Ito, and H. Takagi, Phys. Rev. Lett. **90**, 193201 (2003).
[19] T. Tanabe, K. Noda, M. Saito, E. B. Starikov, and M. Tateno, Phys. Rev. Lett. **93**, 043201 (2004).
[20] D. Zajfman A. Wolf, S. Schwalm, D. A. Orlov, M. Grieser, R. v. Hahn, C. P. Welsch, J. R. C. Lopez-Urrutia, C. D. Schroter, X. Urbain, and J. Ullrich, J. Phys.: Conf. Ser. **4**, 296 (2005).
[21] P. Löfgren, G. Andler, L. Bagge, M. Blom, H. Danared, A. Källberg, S. Leontein, L. Liljeby, A. Paál, K.-G. Rensfeld, A. Simonsson, H. Cederquist, M. Larsson, S. Rosén, H. T. Schmidt, and K. Schmidt, EPAC 2006, Edinburg, United Kingdom, 2006 (unpublished), p. 252.
[22] H. T. Schmidt, H. A. B. Johansson, R. D. Thomas, W. D. Geppert, N. Haag, P. Reinhed, S. Rosén, M. Larsson, H. Danared, K. G. Rensfelt, L. Liljeby, L. Bagge, M. Björkhage, M. Blom, P. Löfgren, A. Källberg, A. Simonsson, A. Paál, H. Zettergren, and H. Cederquist, Int. J. Astrobiology (unpublished).
[23] S. Rosen, H. T. Schmidt, P. Reinhed, D. Fischer, R. D. Thomas, H. Cederquist, L. Liljeby, L. Bagge, S. Leontein, and M. Blom, Rev. Sci. Instrum. **78**, 113301 (2007).
[24] J. Bernard, S. Martin, L. Chen, H. Cederquist, A. Salmoun, and R. Brédy, Nucl. Instrum. Methods Phys. Res. B **205**, 196 (2003).
[25] J. Bernard, B. Wei, A. Bourgey, R. Brédy, L. Chen, M. Kerleroux, S. Martin, G. Montagne, A. Salmoun, and B. Terpend-Ordaciere, Nucl. Instrum. Methods Phys. Res. B **262**, 105 (2007).
[26] S. Tomita, J. U. Andersen, H. Cederquist, B. Concina, O. Echt, J. S. Forster, K. Hansen, B. A. Huber, P. Hvelplund, J. Jensen, B. Liu, B. Manil, L. Maunoury, S. B. Nielsen, J. Rangama, H. T. Schmidt, and H. Zettergren, J. Chem. Phys. **124**, 024310 (2006).
[27] H. Zettergren, M. Alcami, and F. Martin, Phys. Rev. A **76**, 043205 (2007).